Correlation of Annihilation Radiation in Oriented Single Metal Crystals*

STEPHAN BERKO† AND JOHN S. PLASKETT
University of Virginia, Charlottesville, Virginia
(Received July 31, 1958)

Precision measurements of the two-photon annihilation in crystals of Al and Cu are presented. These show relatively small variation with crystal orientation. This is interpreted to mean that the strong high-momentum tail in the Cu distribution is due to annihilation with the 3*d* electrons and that the Fermi surface in Al is very nearly spherical but has slight bulges in the [100] and [111] directions. One-electron calculations of the distributions for Cu and Al agree quite well with the experiments and further confirm the importance of core annihilation in Cu. The calculated positron lifetime in Cu does not disagree with previous experimental observations by more than a factor of two. Electron-positron correlation by any factor much larger than this is therefore precluded.

1. INTRODUCTION

SINCE the first measurements by DeBenedetti *et al.*[1] on the angular distribution of annihilation radiation in Au, a number of investigators have applied the same method to a variety of solids and liquids.[2] It has been pointed out by these workers that a study of annihilation of positrons in metals could provide direct information on the momentum distributions of valence electrons in these metals, since the probability of observing a certain angle between the two annihilation photons depends directly on the square of the Fourier transform of the positron-electron wave function.

Most existing measurements of the angular distributions have been performed on polycrystalline samples,[3] so that only the spherical average of the momentum distributions could be determined. The possibility of measuring momentum anisotropies in oriented single crystals was demonstrated by us in a previous paper on the angular correlation of annihilation radiation in oriented graphite.[4] In this paper we present more recent measurements on single crystals of Cu and Al, to examine how well this technique can be used in the determination of electron properties in metals, particularly the shape of the Fermi surface. The bulk of the paper is, however, of a theoretical nature. Computations are presented in an attempt to explain the details of the measured angular distributions, using computed Hartree-Fock positron wave functions.[5]

2. NATURE OF THE THEORETICAL PROBLEM

There seems to be no doubt that a positron has reached thermal equilibrium in a metal before it annihilates[6] (it has $\sim 10^{-10}$ sec). We may therefore suppose that the electron-positron system annihilates from its ground state. A simple estimate of the positron lifetime using constant positron wave functions and annihilation with the valence electrons only, yields values that are longer and vary more from metal to metal than the measured lifetimes. Calculations have been performed emphasizing the importance of strong correlations between the positron and the electrons.[7] It is well known, however, that many properties of metals can be understood in terms of one-particle—uncorrelated—wave functions, and it seems to be worthwhile to investigate quite thoroughly whether this may not also be true for positron annihilation. Indeed before this is done, it will not really be clear what effects have to be attributed to correlation. For this purpose it is important to make calculations on several metals that have as different angular distributions of the annihilating photons as possible.

Roughly speaking, the angular distributions fall into two classes. There are those that appear very nearly parabolic with a fairly sharp cutoff at an angle θ given by $\hbar k'/mc$, where k' is the wave vector corresponding to the Fermi surface of the valence electrons as calculated by the free electron approximation; the alkalis, alkaline earths, and aluminum are examples. The other class has angular distributions that extend way beyond the expected Fermi cutoff and do not show any prominent break; the noble metals are examples. One example from each class is discussed in this paper: aluminum and copper. DeBenedetti and Primakoff,[1] who first observed the wide angular distribution (in gold), attributed it to the sharp cutoff of the positron wave function at the core of the Au ion. This suggestion of the "excluded volume effect" was again proposed by Ferrell.[7] On the other hand, from an examination of the distributions obtained by Stewart from annihilation in the series Ni, Cu, Zn, and Ga, Berko and Hereford[2] proposed that the large momenta were due to annihilation with the 3*d* electrons.

* The experimental part of this paper was supported by the Office of Naval Research.
† Alfred P. Sloan Research Fellow, 1957–1958.
[1] DeBenedetti, Cowan, Konneker, and Primakoff, Phys. Rev. **77**, 205 (1950).
[2] For references see the review article by S. Berko and F. L. Hereford, Revs. Modern Phys. **28**, 299 (1956).
[3] L. G. Lang and S. DeBenedetti, Phys. Rev. **108**, 914 (1957); A. T. Stewart, Can. J. Phys. **35**, 168 (1957).
[4] Berko, Kelley, and Plaskett, Phys. Rev. **106**, 824 (1957).
[5] Two independent computations on the positron wave function in Cu (see part of our Sec. 4.1) have been recently published: E. Daniel, J. phys. radium **18**, 691 (1957) and B. Donovan and N. H. March, Phys. Rev. **110**, 582 (1958). These authors do not compute the positron annihilation with the Cu core electrons.
[6] G. E. Lee-Whiting, Phys. Rev. **97**, 1557 (1955).
[7] R. A. Ferrell, Revs. Modern Phys. **28**, 308 (1956); E. Daniel and J. Friedel, J. Phys. Chem. Solids **4**, 111 (1958).

It will be shown that, independently from the theoretical computations (that clearly indicate that the excluded volume effect is too small and that $3d$ annihilation is quite adequate to account for the large momenta) one can distinguish experimentally between core annihilation *vs* "excluded volume effect" by doing angular correlation experiments on oriented crystals of copper. This then was another reason (besides that outlined in the Introduction) for performing experiments on oriented metal crystals.

After a brief discussion in Sec. 3, of the experimental setup and procedure, the details of the theoretical computations are described in Sec. 4. The results of this computation are then discussed and compared with the new experimental data in the final paragraph of this paper.

3. EXPERIMENTAL SETUP AND PROCEDURE

Let $\Gamma(\mathbf{p})d\mathbf{p}$ be the probability that a positron annihilates with an electron via two photons having total momentum between $\mathbf{p}$ and $\mathbf{p}+d\mathbf{p}$ in the laboratory system of coordinates. This momentum $\mathbf{p}$ is then directly related to the angle of emission between the two photons. Two kinds of angular correlation setups have been described in the past to obtain a measure of $\Gamma(\mathbf{p})$. In the setup as used by DeBenedetti *et al.*,[1] two parallel slits are used as collimators in front of the photon counters; the angular distribution thus measured is

$$F_z(\theta)=A\int_{-\infty}^{\infty}\int_{-\infty}^{\infty}\Gamma(p_x,p_y,mc\theta)dp_xdp_y,$$

where the integration is in rectangular coordinates (x, y, z). A is a normalization constant.

More recently a cylindrical geometry has been used independently by Millett[8] and Hannah.[9] One collimator defines a narrow cone originating at the sample, while the other defines a thin conical shell between θ and $\theta+d\theta$ coaxial with the cone defined by the first. Thus the angular distribution obtained by varying the aperture of the second collimator measures

$$G_r(\theta)=B\int_{-\infty}^{\infty}\int_{0}^{2\pi}\Gamma(p_x,p_\varphi,mc\theta)dp_xdp_\varphi,$$

in a cylindrical system of coordinates (x, φ, r).

Despite some advantages of the cylindrical setup as outlined by Millett, we decided to use the parallel slit system for the following reasons: (*a*) We wanted to have an automatic setup in order to be able to take data over long periods of time; the parallel slit can be moved on an arm, thereby changing θ without disturbing the angular resolution, instead of having to insert a new conical collimator for each angle. (*b*) When oriented single crystals are used and the momentum distribution is not isotropic, a plane geometry that conforms to the crystalographic planes is easier to interpret than a cylindrical geometry.

The experimental setup was very similar to that described by Lang.[3] It consisted of a positron source shielded by lead, a target holder, a stationary and a moving counter and the associated collimators. The positron source was 4–5 mC of Na^{22} deposited in a stainless steel cup and covered with a thin Mylar window. The steel cup was inserted in the face of a lead brick that served as a source holder and shield. The target holder consisted of a precision turret which could hold four different metal samples that could be rotated, one at a time, with their flat faces parallel to the Mylar window of the source. This setup allowed one to change to various crystalline faces without removing the Na^{22} source. The turret was mounted on a micrometer screw used to adjust with precision the distance between the source and the sample. All metal samples were 0.5-inch diam cylinders. The single-crystal samples were grown for us by the Virginia Institute for Scientific Research, Richmond, Virginia, and were oriented within $\pm 0.5°$ with their crystallographic axis parallel to the axis of the cylinders. This orientation and also the condition of the surface was reached by standard x-ray techniques.

The scintillation detectors consisted of $1\times15\times15$ cm slabs of NE102 plastic scintillator mounted on Lucite light pipes. The light pipe was designed to couple efficiently to the 1.5-inch diam circular face of the photomultiplier tube (RCA 6342), operated at 1250 volts. The two counter assemblies rested on two horizontal steel arms pivoted under the sample. The slits in front of the counters had machined lead faces and subtended an adjustable angle $\Delta\theta$ to the sample. In the measurements on Al we used an angle of 0.56 milliradian; for the Cu curve 1.1 milliradians was used.

The electronics consisted of a standard coincidence setup having 10^{-7} sec resolving time. Much care was taken to use ultrastabilized components in view of the long time that was necessary to accumulate counts. The whole apparatus was made fully automatic, the moving arm being mounted in a carriage moved by a precision screw driven by a motor; this was activated at the end of each preset count cycle. The stops of the carriage could be adjusted to every half or every full milliradian. The whole range of the angular distribution curve was adjustable by properly spaced reversing microswitches. The data were printed in terms of elapsed time, thus furnishing counting rate *vs* angle with points having constant preset statistics.

The various factors that enter the geometrical resolution have been discussed at length by Lang.[10] With the large scintillators used, the vertical resolution could

[8] W. E. Millett and R. Castillo-Bahena, Phys. Rev. **108**, 257 (1957).
[9] S. S. Hannah and R. S. Preston, Phys. Rev. **109**, 716 (1958).
[10] L. G. Lang, Ph.D. dissertation, Carnegie Institute of Technology, 1956 (unpublished).

be made much larger than the widths of the distribution curves measured, thus justifying the integration of $\Gamma(\mathbf{p})$ from $-\infty$ to $+\infty$ along the vertical direction. The angular resolution curve in the horizontal direction could be approximated by a triangle of base twice the width of the individual slits. Data were taken at stops of 400–1000 counts at each point, recycling several times over the preset range, and averaging the results. Counting rates as high as 100 counts a minute could be obtained at 0° with the 1.1-milliradian resolution. The background, measured by moving the arm to 30 milliradians, did not exceed in any of the runs one percent of the counting rate at 0°. The measured angular distribution curves will be presented in Sec. 5 together with the theoretical results.

4. CALCULATIONS

4.1 Calculation of the Positron Wave Function

The ground state of the positron will be at the bottom of a $1s$ band, $\mathbf{k}=\mathbf{0}$. Thermal excitation is irrelevant. The Wigner-Seitz method was used to calculate this wave function, $\psi_+(\mathbf{r})$. Inside the cell centered at the origin, $\psi_+=R_+(r)/r$ and R_+ satisfies[11]

$$R_+''+[E+2V(r)]R_+=0.$$

$V(r)$ was taken to be the potential of the positive ion Cu^+ or Al^{+3},[12] together with the potential due to a uniform charge distribution of one or three electrons per atom. The radial wave equation was integrated out from the origin in the usual way[13] and E was chosen to fit the boundary condition $(R_+/r)'=0$ at $r=r_s$, the radius of the Wigner-Seitz sphere: 2.67 atomic units in Cu and 2.98 atomic units in Al. The eigenvalues found

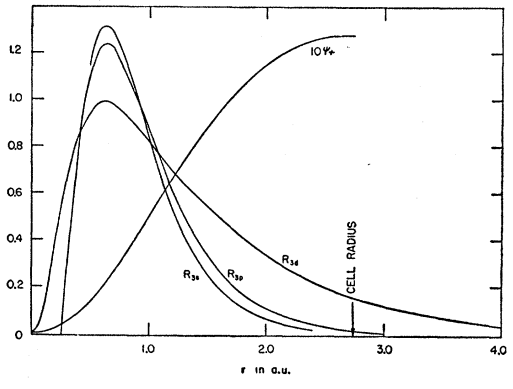

FIG. 1. The normalized positron wave function ψ_+ and the normalized radial wave functions for the M shell of Cu.

[11] Atomic units (a.u.) are used except that E is measured in rydbergs. Note that, in a.u., $m=e=\hbar=1$ and $c=137$.

[12] For Cu^+ with exchange this is given by D. R. Hartree and W. Hartree, Proc. Roy. Soc. (London) **A157**, 490 (1936); without exchange it is given by D. R. Hartree, Proc. Roy. Soc. (London) **A141**, 282 (1933). For Al^{+3} with exchange it was computed from the tables of C. Froese, Proc. Cambridge Phil. Soc. **53**, 206 (1957).

[13] D. R. Hartree, *Numerical Analysis* (Clarendon Press, Oxford, 1952), Sec. 7.2.

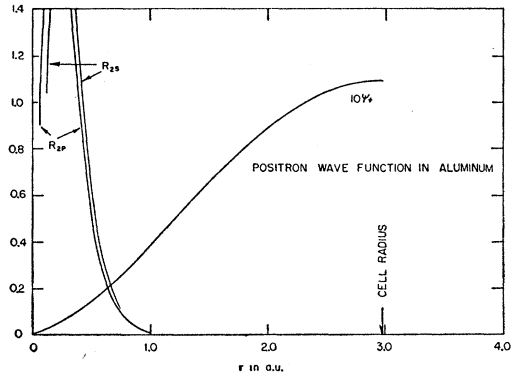

FIG. 2. The normalized positron wave function ψ_+ and the normalized radial wave functions for the L shell of Al.

were +0.395 ry and +0.515 ry in Cu with and without exchange, respectively and +0.355 ry in Al. $10\psi_+$ with exchange is plotted for Cu, Fig. 1, and for Al, Fig. 2. ψ_+ without exchange was originally worked out for Cu by Garofalo[14] and is not very different from ψ_+ with exchange. ψ_+ has been normalized to 1 in a single cell.

4.2 Calculation of the Momentum Distribution of the Ions

The wave functions for the core electrons in Cu^+ and Al^{+3} are given by Hartree and Hartree and Froese.[15] The radial functions $R(r)$ for the M shell of copper (with exchange) and the L shell of aluminum are plotted in Figs. 1 and 2, respectively. These radial functions are normalized so that $\int_0^\infty R^2dr=1$. If we neglect overlap of wave functions on different atoms, the positron-electron momentum distribution corresponding to the $2(2l+1)N$ core functions of angular momentum l on the N atoms of the crystal is

$$\rho_l(\mathbf{p})=2N\sum_{m=-l}^{l}\left|\int_{\text{crystal}}(N^{-\frac{1}{2}}\psi_+)(R_l/r)Y_l^m e^{-i\mathbf{p}\cdot\mathbf{r}}d\mathbf{r}\right|^2, \quad \text{(A)}$$

where

$$\frac{1}{r}Y_l^m=\frac{1}{r}P_l^m e^{im\varphi}\left(\frac{2l+1}{4\pi}\frac{(l-m)!}{(l+m)!}\right)^{\frac{1}{2}}$$

is a normalized core electron wave function and $N^{-\frac{1}{2}}\psi_+$ is the normalized positron wave function. The integrand of the above integral is very small outside the central cell and inside $\psi_+=R_+/r$ is spherically symmetrical. For the small contribution to the integral outside the cell we have replaced ψ_+ by its spherically symmetrical average, $\bar{\psi}_+$, computed from the Fourier series for ψ_+ (see Sec. 4.3). It may seem inconsistent to use the atomic wave functions as if there were no overlap and then bother about the contribution to the momentum

[14] A. M. Garofalo, Ph.D. dissertation, University of Virginia, 1957 (unpublished). See also reference 5.

[15] See papers under reference 12.

distribution where the atomic functions do overlap. Even if there is overlap the expression A can be justified, however, by the use of the tight-binding approximation provided the normalization overlap integrals are neglected (see 4.3). The expression A with ψ_+ replaced by $\bar{\psi}_+$ can easily be summed over m and integrated over φ and θ. The result is

$$\rho_l(p)=4\pi\times 2(2l+1)\left[\int_0^\infty r\bar{\psi}_+R_l\left(\frac{\pi}{2pr}\right)^{\frac{1}{2}}J_{l+\frac{1}{2}}(pr)dr\right]^2.$$

This integral has been evaluated numerically for the various l of the M shell for Cu and the L shell for Al. The inner shells produce effectively no contribution because of the small electron-positron overlap for them. The results are shown in Figs. 3 and 4. In Fig. 3 for Cu the ρ_{3d} calculated from the positron wave function without exchange and the $3d$ wave function without exchange is shown (ρ_{3d}'). The reason for the large difference between ρ_{3d} and ρ_{3d}' is largely due to the fact that the $3d$ function without exchange extends farther than the $3d$ with exchange. This is not compensated by the fact that the positron with exchange enters deeper into the core. We have not bothered to show ρ_{3s}' and ρ_{3p}', the momentum distribution, of the $3s$ and $3p$ electrons without exchange; they do not differ from ρ_{3s} and ρ_{3p} by more than 10%.

4.3 Calculation of the Momentum Distribution for Bloch Functions

The momentum distribution due to annihilation with a doubly occupied Bloch function $e^{i\mathbf{k}\cdot\mathbf{r}}u_{\mathbf{k}}(\mathbf{r})N^{-\frac{1}{2}}$, where $u_{\mathbf{k}}$ is normalized to 1 inside a cell, is

$$\rho_{\mathbf{k}}(\mathbf{p})=2\left|\int_{\text{crystal}}N^{-\frac{1}{2}}e^{i\mathbf{k}\cdot\mathbf{r}}u_{\mathbf{k}}N^{-\frac{1}{2}}\psi_+e^{-i\mathbf{p}\cdot\mathbf{r}}d\mathbf{r}\right|^2.$$

If we imagine that the quantization of the radiation field is made in a box much larger than the size of the crystal, $\mathbf{p}$ will be effectively a continuous variable compared to the variable $\mathbf{k}$ that can only take on discrete values. This integral is very nearly zero unless $\mathbf{k}-\mathbf{p}$ is a reciprocal lattice vector of the crystal. We can evaluate the integral in the usual way: $u_{\mathbf{k}}$ and ψ_+ are periodic with the periods $\boldsymbol{\tau}$, the lattice vectors of the crystal; therefore

$$\rho_{\mathbf{k}}(\mathbf{p})=2\left|\left(\frac{1}{N}\sum_{\boldsymbol{\tau}\,\text{crystal}}\exp[i(\mathbf{k}-\mathbf{p})\cdot\boldsymbol{\tau}]\right)\times\int_{\text{cell}}e^{i(\mathbf{k}-\mathbf{p})\cdot\mathbf{r}}u_{\mathbf{k}}\psi_+d\mathbf{r}\right|^2.$$

The sum over $\boldsymbol{\tau}$ can be easily performed and is indeed a function of $\mathbf{p}$ with strong maxima at the points $\mathbf{k}+\boldsymbol{\alpha}$, where $\boldsymbol{\alpha}$ is an arbitrary reciprocal lattice vector. The value of the sum at its maxima is N and the width of a maximum is of order $N^{-\frac{1}{3}}$. The fine structure in $\rho_{\mathbf{k}}(\mathbf{p})$ is unimportant and all we are interested in is the integral of $\rho_{\mathbf{k}}(\mathbf{p})$ over a region containing one maximum, say the region round $\mathbf{p}=\mathbf{k}+\boldsymbol{\alpha}$. After integrating the sum with respect to $\mathbf{p}$, we find

$$\int_{\mathbf{k}+\boldsymbol{\alpha}}\rho_{\mathbf{k}}(\mathbf{p})d\mathbf{p}=2\frac{(2\pi)^3}{N\Omega}|A_\alpha(\mathbf{k})|^2,$$

where

$$A_\alpha(\mathbf{k})=\int_{\text{cell}}\exp(-i\boldsymbol{\alpha}\cdot\mathbf{r})u_{\mathbf{k}}\psi_+d\mathbf{r}$$

and Ω is the volume of a cell. This can be picturesquely described as follows: The momentum distribution of the photon pair coming from an annihilation of an electron in the state described by the wave vector $\mathbf{k}$ is a set of δ functions situated at the points $\mathbf{k}+\boldsymbol{\alpha}$ with relative weights $|A_\alpha|^2$, i.e.,

$$\rho_{\mathbf{k}}(\mathbf{p})=2\frac{(2\pi)^3}{N\Omega}\sum_\alpha|A_\alpha(\mathbf{k})|^2\delta[\mathbf{p}-(\mathbf{k}+\boldsymbol{\alpha})],$$

where δ is an approximation to the Dirac δ function of width $N^{-\frac{1}{3}}$. To obtain the total momentum distribution of all the occupied Bloch functions, we must sum $\rho_{\mathbf{k}}(\mathbf{p})$ over the occupied states $\mathbf{k}$:

$$\sum_{\mathbf{k}}\rho_{\mathbf{k}}(\mathbf{p})=\int\rho_{\mathbf{k}}(\mathbf{p})\frac{N\Omega}{(2\pi)^3}d\mathbf{k},$$

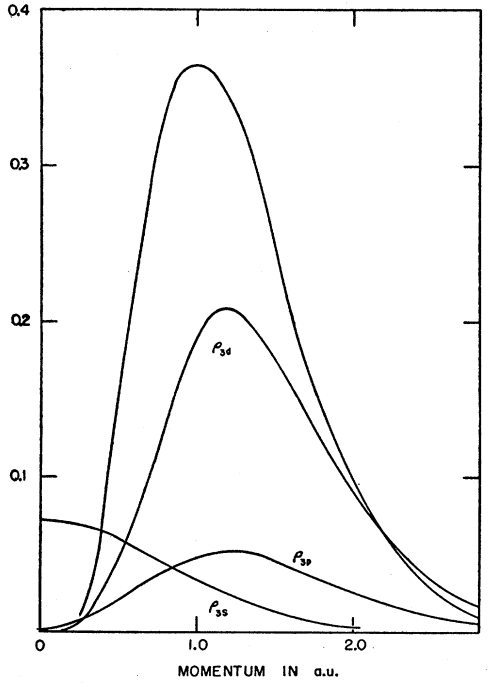

FIG. 3. Momentum distributions of the wave function products for the M-shell electrons in Cu, ρ_{3s}, ρ_{3p}, and ρ_{3d} with exchange, ρ_{3d}' without exchange. ρ_{3d}' is the unmarked curve.

where the integral is taken inside the Fermi surface and the factor $N\Omega/(2\pi)^3$ is the density of eigenstates, $\mathbf{k}$, in the wave vector space. We find

$$\sum_{\mathbf{k}} \rho_{\mathbf{k}}(\mathbf{p}) = 2|A_\alpha(\mathbf{p}-\boldsymbol{\alpha})|^2 \quad \text{or} \quad 0$$

according as there is or is not a reciprocal lattice vector $\boldsymbol{\alpha}$ that makes $\mathbf{p}-\boldsymbol{\alpha}$ lie inside the occupied region of the wave-vector space.

Tightly Bound Electrons

Let us apply this result to the Bloch tight-binding functions in which

$$e^{i\mathbf{k}\cdot\mathbf{r}}u_{\mathbf{k}}(\mathbf{r}) = \sum_\tau \exp(i\mathbf{k}\cdot\boldsymbol{\tau})\varphi(\mathbf{r}-\boldsymbol{\tau}),$$

where $\varphi(\mathbf{r})$ is a normalized atomic function and, in order that we should have the Bloch function correctly normalized, the overlap integrals have the property

$$\int \varphi^*(\mathbf{r})\varphi(\mathbf{r}-\boldsymbol{\tau})d\mathbf{r} \ll 1, \quad \boldsymbol{\tau} \neq \mathbf{0}.$$

It is readily verified that for this Bloch function

$$A_\alpha(\mathbf{k}) = \int_{\text{space}} \exp[-i(\boldsymbol{\alpha}+\mathbf{k})\cdot\mathbf{r}]\varphi(\mathbf{r})\psi_+(\mathbf{r})d\mathbf{r}.$$

If we have a full zone, then it will always be possible to find an $\boldsymbol{\alpha}$ such that $\mathbf{p}-\boldsymbol{\alpha}$ is inside the occupied region and we return to our formula in Sec. 4.2:

$$\rho_\varphi(\mathbf{p}) = 2|A_\alpha(\mathbf{p}-\boldsymbol{\alpha})|^2 = N\left|\int e^{-i\mathbf{p}\cdot\mathbf{r}}\varphi(\mathbf{r})\psi_+(\mathbf{r})N^{-\frac{1}{2}}d\mathbf{r}\right|^2.$$

Nearly Free Electrons

As another interesting example let us calculate what the momentum distribution should look like for electrons that are close to a zone face. This should presumably be important for the hexagonal face of copper[16]

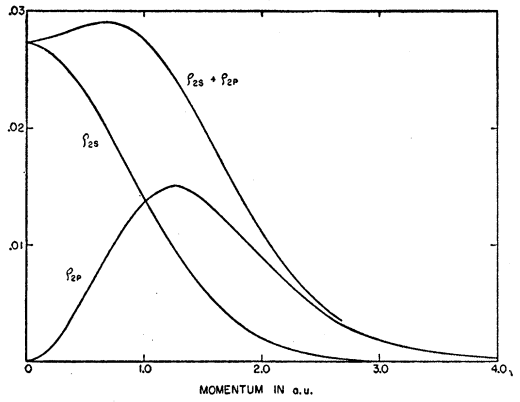

FIG. 4. Momentum distributions of the wave-function products for the L-shell electrons in Al.

[16] H. Jones, Proc. Phys. Soc. (London) **A68**, 1191 (1955). A. B. Pippard, Trans. Roy. Soc. (London) **A250**, 325 (1957).

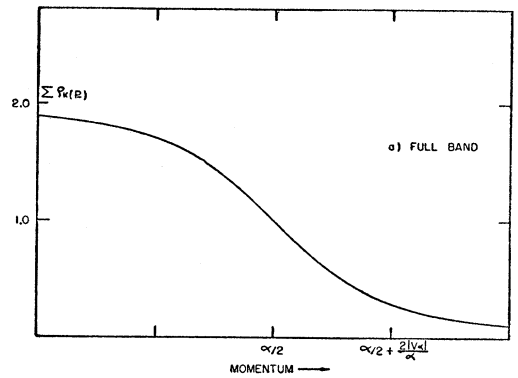

FIG. 5. Angular distribution near a zone face ($\alpha/2$) computed in the "nearly free electron" approximation. The energy gap is $4|V_\alpha|$ ry. Fermi surface at zone face.

and of course occurs in aluminum. To get a rough idea of the magnitude of the effect, we use the nearly free electron approximation.[17] When $\mathbf{k}$ is near the zone face defined by the plane $\mathbf{k}\cdot\boldsymbol{\alpha} = \alpha^2/2$, the Bloch wave function is

$$e^{i\mathbf{k}\cdot\mathbf{r}}[B_0(\mathbf{k}) + B_\alpha(\mathbf{k})\exp(-i\boldsymbol{\alpha}\cdot\mathbf{r})],$$

where B_0 and B_α are determined by the secular equation

$$\begin{bmatrix} k^2+2V_0-E & 2V_{-\alpha} \\ 2V_\alpha & (\mathbf{k}-\boldsymbol{\alpha})^2+2V_0-E \end{bmatrix}\begin{bmatrix} B_0(\mathbf{k}) \\ B_\alpha(\mathbf{k}) \end{bmatrix} = 0.$$

The energy gap between the two bands given by this equation is $4|V_\alpha|$ ry at the zone face. If we define x by the equation

$$(\tfrac{1}{2}\boldsymbol{\alpha}-\mathbf{k})\cdot\boldsymbol{\alpha} = 2|V_\alpha|x,$$

so that x is proportional to the distance of $\mathbf{k}$ from the zone face, then

$$\begin{bmatrix} |B_0^\pm(\mathbf{k})|^2 \\ |B_\alpha^\pm(\mathbf{k})|^2 \end{bmatrix} = \begin{bmatrix} \frac{1}{2} \mp \frac{1}{2}x(1+x^2)^{-\frac{1}{2}} \\ \frac{1}{2} \pm \frac{1}{2}x(1+x^2)^{-\frac{1}{2}} \end{bmatrix}.$$

The upper and lower signs refer to the upper and lower bands, respectively. If we assume that the positron wave function is a constant, $|B_0|^2$ and $|B_\alpha|^2$ will give the momentum distributions of the photon pair produced on annihilation. The distributions when (*a*) the lower band is filled up to the zone face, (*b*) the lower band is not quite filled, and (*c*) there is overflow into the upper band are shown in Figs. 5, 6, and 7, respectively. In the examples (*b*) and (*c*) the wave vector corresponding to the Fermi surface was taken as $\frac{1}{2}\alpha - |V_\alpha|/\alpha$. It will be observed that when the Fermi surface is bigger than $4|V_\alpha|/\alpha$ away from the zone face, the momentum distribution is within 5% of its constant free electron value. Furthermore an insulator should show no sharp breaks in its momentum distribution.

[17] N. F. Mott and H. Jones, *Properties of Metals and Alloys* (Clarendon Press, Oxford, 1936), p. 61.

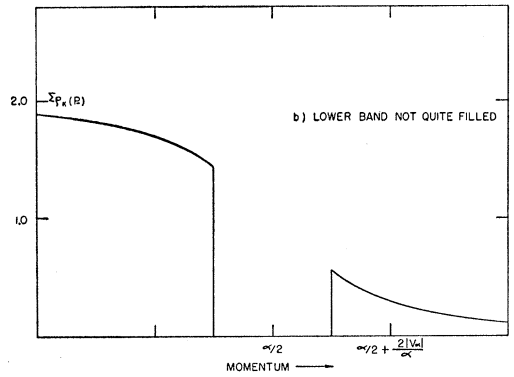

FIG. 6. Angular distribution near a zone face ($\alpha/2$) computed in the "nearly free electron" approximation. The energy gap is $4|V_\alpha|$ ry. Fermi surface below zone face.

Wigner-Seitz Electrons

Since the correct $u_0(\mathbf{r})$ is known by a Wigner-Seitz calculation, it is possible to see what the momentum distribution is for annihilation with the valence electrons near $\mathbf{k}=\mathbf{0}$. The momentum distribution at the point $\mathbf{p}=\boldsymbol{\alpha}$ is

$$2|A_{\mathbf{p}}(\mathbf{0})|^2=2\left|\int_{\text{cell}} e^{-i\mathbf{p}\cdot\mathbf{r}}u_0\psi_+ d\mathbf{r}\right|^2.$$

Some caution must be exercised in evaluating this integral. It is quite incorrect to replace the region of integration by the Wigner-Seitz sphere. We write

$$\int_{\text{cell}} e^{-i\mathbf{p}\cdot\mathbf{r}}u_0\psi_+ d\mathbf{r}$$

$$=\int_{\text{cell}} e^{-i\mathbf{p}\cdot\mathbf{r}}(u_0\psi_+-u_0'\psi_+')d\mathbf{r}+u_0'\psi_+'\Omega\delta_{\mathbf{p},0},$$

where $u_0'\psi_+'$ is just the value of $u_0\psi_+$ at the Wigner-Seitz radius. The integrand of the integral on the right is now zero and has a zero derivative at the Wigner-Seitz radius and we replace the region of integration by a sphere in *this* integral. The values of $A_\alpha(\mathbf{0})$ computed in this way for Cu are shown in Table I for the first four shells of $\boldsymbol{\alpha}$'s surrounding $\boldsymbol{\alpha}=\mathbf{0}$. It is seen that the momentum distribution due to the electrons near $\mathbf{k}=\mathbf{0}$ is almost all concentrated at $\mathbf{p}=\mathbf{0}$. In fact the proportion of the momentum outside the Fermi surface to the whole distribution (for $\mathbf{k}=\mathbf{0}$ electrons) is

$$\sum_{\alpha\neq 0}|A_\alpha|^2/\sum_\alpha|A_\alpha|^2=0.193/1.101=0.175.$$

If all the copper valence electrons behaved in this way they would give rise to a momentum distribution 18% of which would be outside the Fermi surface. The angular distribution computed as though $|A_\alpha(\mathbf{k})|^2=|A_\alpha(\mathbf{0})|^2$ for all electrons in the Fermi surface is shown for various orientations in Fig. 8. For the method of computation see Sec. 5. Part of the high momentum distribution of this figure can be attributed to the "excluded volume effect." The fact that along the [110] direction this distribution shows a secondary maximum can be used to check independently by experiment the assumption that the large momenta in copper are due entirely to this effect. The area under this distribution

TABLE I. Table of Fourier components. (Σ^4 means the summation over the first four shells of $\boldsymbol{\alpha}$'s surrounding $\alpha=0$.)

$(2\pi/a)\boldsymbol{\alpha}$	[000]	[111]	[200]	[220]	[311]	$\Omega\Sigma^4\|B_\alpha\|^2$
$A_\alpha(\mathbf{0})$	0.953	−0.127	−0.087	−0.009	+0.006	
$B_\alpha{}^+$	0.1086	−0.0077	−0.0055	−0.0010	−0.0001	0.994
$B_\alpha{}^-(\mathbf{0})$	0.0983	−0.0140	−0.0110	−0.0041	−0.0019	0.976
$\tilde{A}_\alpha(\mathbf{0})$	0.953	−0.128	−0.088			
$B_\alpha{}^F$	0.0915	−0.0164	−0.0105	+0.0018	+0.0039	0.925

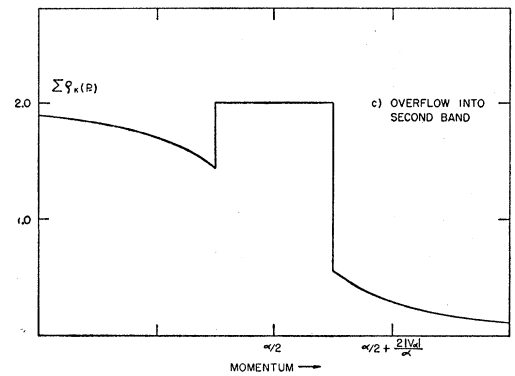

FIG. 7. Angular distribution near a zone face ($\alpha/2$) computed in the "nearly free electron" approximation. The energy gap is $4|V_\alpha|$ ry. Fermi surface above zone face.

is in itself of course much too small to explain the experimental copper curve. Of course electrons near a zone face must be expected to give a bigger contribution outside the Fermi surface, as we saw in the free electron approximation. This 18% figure is therefore presumably an underestimate.

It is interesting to inquire into the relative importance of the electron and the positron in producing these high momenta. In the same Table I we show the Fourier components of the positron and electron (upper and lower signs, respectively):

$$B_\alpha{}^\pm=\Omega^{-1}\int_{\text{cell}}\exp(-i\boldsymbol{\alpha}\cdot\mathbf{r})\psi_\pm d\mathbf{r}.$$

We can check these integrals since we must have $\Omega\sum|B_\alpha|^2=1$ by Parseval's theorem. Similarly we should have $A_\alpha=\Omega\sum_{\alpha'}B_{\alpha'}{}^+B_{\alpha-\alpha'}{}^-$. The sum on the right, called $\tilde{A}_\alpha$, is also shown in the table. All these checks are adequately satisfied. The answer to our question seems to be that the electron plays a bigger role than the positron (by a factor of four); in fact,

$$\Omega\sum_{\alpha\neq 0}|B_\alpha{}^+|^2=0.059,\quad \Omega\sum_{\alpha\neq 0}|B_\alpha{}^-|^2=0.230.$$

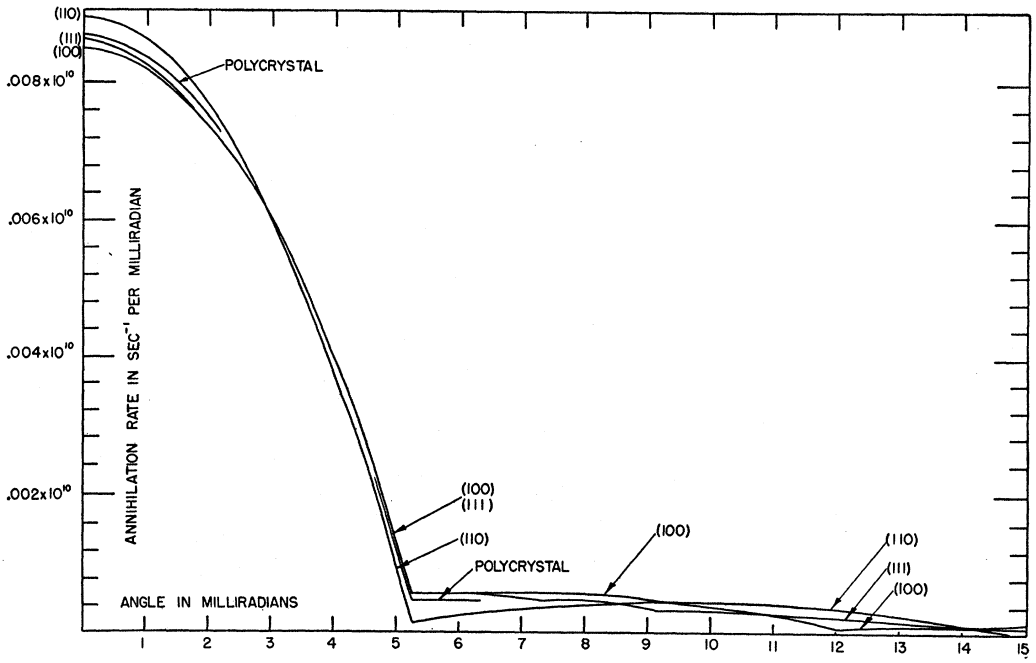

FIG. 8. Calculated angular distribution from annihilation with the 4*s* electrons in Cu for various orientations and also for a polycrystal.

DeBenedetti *et al.* and Ferrell have proposed that the momentum components might be entirely due to the positron with a plane-wave electron. They used a positron wave function that was zero inside some radius r_0 and was a constant everywhere else. In the same table we show the Fourier coefficients, B_α^F, of this function normalized to 1 in the unit cell and with $r_c=1.85$ atomic units (Ferrell's value for Cu). It is seen that this positron wave function gives bigger Fourier components than the 4*s* electron. It is clearly a much better approximation to imagine the positron wave function to be a constant. It is to be noticed that Ferrell thought that this positron wave function would explain the observed high-momentum components in Cu. However, this is not so because

$$\frac{|B_0^F|^2}{\sum_\alpha |B_\alpha^F|^2}=1-\frac{\Omega_c}{\Omega},$$

not $(1-2\Omega_c/\Omega)/(1-\Omega_c/\Omega)$ as stated by Ferrell [Eq. (26)]. Here $\Omega_c=4\pi r_c^3/3$.

We have not thought that it was worth while to do similar calculations for Al because of the limited number of valence electrons near $\mathbf{k}=\mathbf{0}$.

It is a very obvious fact, but is perhaps worth pointing out, that

$$|A_\alpha(\mathbf{k})|^2=\left|\int \exp(-i\boldsymbol{\alpha}\cdot\mathbf{r})u_{\mathbf{k}}\psi_+ d\mathbf{r}\right|^2\leqslant 1,$$

by Schwartz's inequality. As we have seen, this upper limit on the momentum distribution for any electrons is very nearly attained (within 9%) by the valence electrons near $\mathbf{k}=\mathbf{0}$ for the momentum $\mathbf{p}=\mathbf{0}$.

5. RESULTS AND DISCUSSION

The momentum distribution of the electron-positron product wave function that we have worked out in the preceding sections gives directly the annihilation rate of the particular electron considered. In fact, if the normalized electron (doubly occupied) and positron wave functions are ψ_i and ψ_+, then the annihilation rate into the momentum region $d\mathbf{p}$ centered at $\mathbf{p}$, is

$$\Gamma_i(\mathbf{p})d\mathbf{p}=\frac{\alpha^3}{4\pi^2}\left|\int \psi_i(\mathbf{r})\psi_+(\mathbf{r})e^{-i\mathbf{p}\cdot\mathbf{r}}d\mathbf{r}\right|^2 d\mathbf{p}=\frac{\alpha^3}{8\pi^2}\rho_i(\mathbf{p})d\mathbf{p},$$

where α is the fine structure constant and the rate is in atomic units (the atomic unit of time is 2.42×10^{-17} sec). The annihilation rate into any momentum is

$$\Gamma_i=\frac{\alpha^3}{8\pi^2}\int \rho_i(\mathbf{p})d\mathbf{p}=2\pi\alpha^3\int |\psi_i|^2|\psi_+|^2 d\mathbf{r}.$$

Now the angular distribution measures, as outlined in Sec. 3, the rate of annihilation $F_z(\theta)d\theta$ (the actual measured distribution is of course an arbitrary counting rate) into the momentum region between the planes defined by $p_z=c\theta$ and $p_z+dp_z=c(\theta+d\theta)$, i.e.,

$$F_z(\theta)=\sum_i c\int\int \Gamma_i(p_x,p_y,c\theta)dp_x dp_y.$$

Clearly $\Gamma_i=\int F_{zi}d\theta$ is the total annihilation rate for the wave function ψ_i.

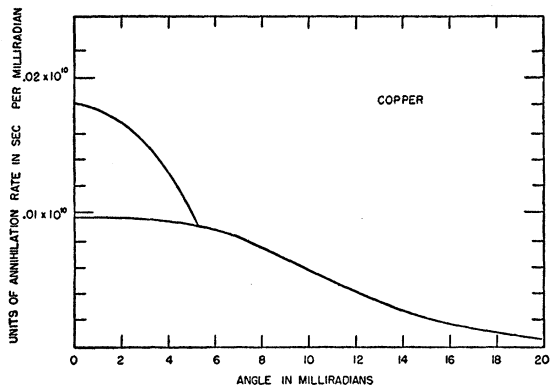

FIG. 9. Calculated angular distribution in Cu. Lower curve for the M-shell electrons (with exchange); upper curve for the $4s$ electrons.

This integration has been carried out numerically for the $\Gamma(\mathbf{p})$ as computed in Sec. 4. The final results have been plotted in units of sec^{-1} per milliradian in Figs. 9 and 10. It is evident that twice the area under the curves (for θ and $-\theta$) is directly the predicted annihilation rate in sec^{-1}. These curves are in reasonable agreement with experiment, as will be shown later. It is to be emphasized that no adjustable parameter has been introduced in the computations. The calculations show therefore that annihilation does occur with the outer shell of the metal ion (the M shell of Cu and the L shell of aluminum) and that this annihilation is mainly responsible for the very broad part of the angular distributions. Superimposed on this broad distribution is the parabolic distribution due to annihilation with the valence electrons which is very prominent in aluminum and less significant in copper. At this point it is worth while checking the annihilation rates predicted from the area of the distribution curves. The introduction of large correlations between positrons and electrons was done[7] because of the discrepancy of the measured rate and those computed by assuming constant positron wave functions and annihilation with n free electrons per atom. This rate is given by

$$\pi\alpha^3 n/\Omega,$$

where Ω is the atomic volume, and α is the fine structure constant. For Al this rate is 0.14×10^{10} sec^{-1}; for Cu it is 0.063×10^{10} sec^{-1}. The calculated area for the L shell in Al is small compared with the area of the parabola, but for Cu the area for the M shell is about four times the area of the parabola; this makes our computed total annihilation rate for Cu about 0.3×10^{10} sec^{-1}. The experimental values for the annihilation rates are $(1.0\pm0.5)\times10^{10}$ sec^{-1} (Bell and Graham)[18] and $(0.37\pm0.04)\times10^{10}$ sec^{-1} (Gerholm[19]) for any metal. Nothing very conclusive can be said about the agreement between these calculated and experimental rates. It is evident that more precise experimental values are needed. It does seem clear, however, that the enhancement of the valence electron rate in copper by a factor 23, as calculated by Daniel and Friedel,[7] is too high. Furthermore, there must be the same order-of-magnitude correlation between the positron and the valence electrons and the positron and the M(Cu) and L(Al) electrons; otherwise the shapes of the angular distributions will be destroyed.

Our conclusion that electron-positron correlation must be very small in copper is entirely dependent on attributing most of the annihilation to the M-shell electrons. If an explanation of the broad angular distribution could be found in terms of annihilation with the valence electrons only, and if, in addition, it could be shown that we have tremendously overestimated annihilation with the M shell (for example because we took the free-ion $3d$ wave functions), then it would be necessary to introduce a large correlation.

This hypothesis is, however, untenable. The high-momentum components due to annihilation with the $4s$ electron (present due to the nonconstancy of the positron wave function or to the $4s$ electron not being a plane wave) can only lie inside the Fermi surface or inside translations of the Fermi surface by reciprocal lattice vectors (that the possible momenta of a wave function in a periodic potential must differ by reciprocal lattice vectors is a statement of Bloch's theorem). This means that the only "occupied" regions of momentum space are a set of nonoverlapping spheres (roughly) of radius $(5.25\times10^{-3}\ mc)$ that are centered at reciprocal lattice points. Now if the copper crystal is oriented so that the [110] component of the momentum is measured, then out to $(5.25\times10^{-3}\ mc)$ we cut through one set of spheres, and from $(4.25\times10^{-3}\ mc)$ to $(14.75\times10^{-3}\ mc)$ we cut through another set, and so on. With the [110] orientation we should therefore see a minimum in the angular distribution at about 5 milliradians and a maximum at about 9 milliradians. Furthermore these

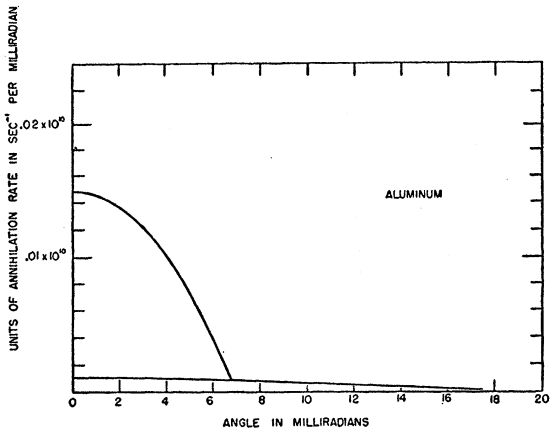

FIG. 10. Calculated angular distribution in Al. Lower curve for the L-shell electrons (with exchange), upper curve for the three valence electrons.

[18] R. E. Bell and R. L. Graham, Phys. Rev. **90**, 644 (1953).
[19] T. R. Gerholm, Arkiv Fysik **10**, 523 (1956).

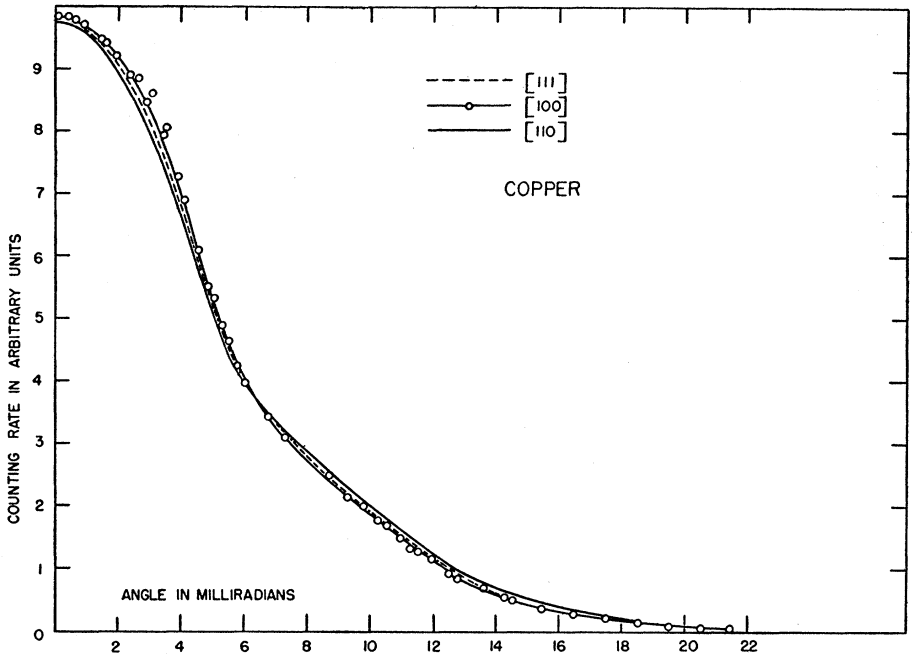

FIG. 11. Experimental angular distributions in Cu oriented along the [111], [110], and [100] directions. The experimental points are included only for the [100] curve.

maxima and minima should shift with crystal orientation (the maxima are farthest apart with the [110] direction and so should be easiest to detect in that direction, e.g., they are only 4 milliradians apart in the [111] direction). See also Sec. 4.3 and Fig. 8.

We have measured the angular distribution from the [111], [100], and [110] in copper out to 25 milliradians. The distributions obtained are plotted in Fig. 11. It is evident that within approximately 5% the angular distributions are the same and that no large secondary maximum is observed around 9 milliradians for the [110] direction. These results rule out the excluded volume effect on purely experimental grounds. The difference between the [110] and the [100] curves does seem to indicate a slight hump at these angles; this effect, if real, would be the reflection of the small

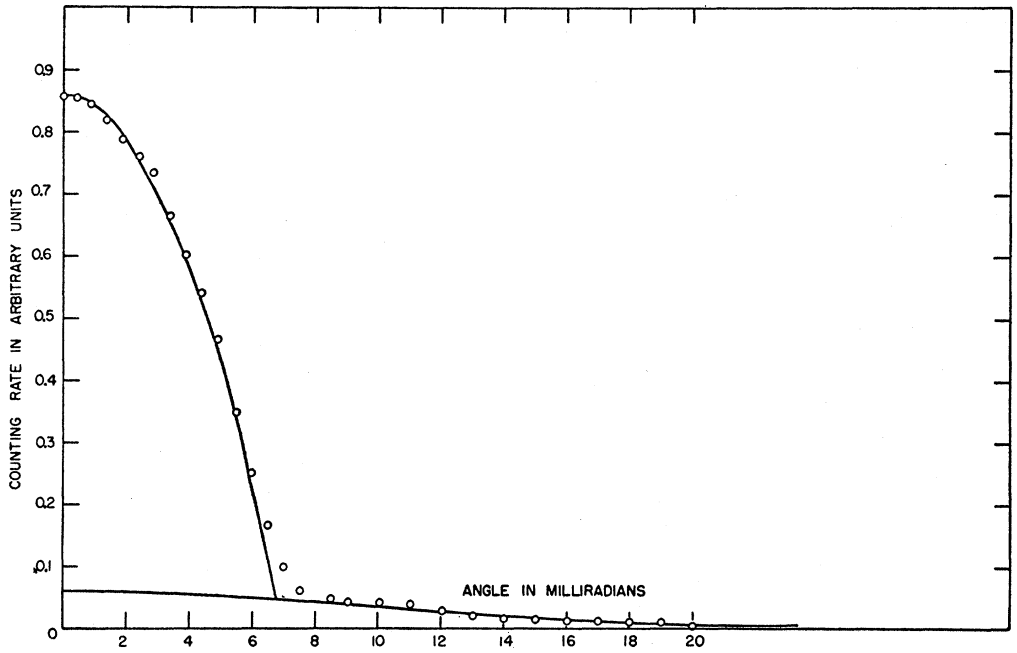

FIG. 12. Angular distribution for aluminum. The points are the experimental points for the [111] direction in aluminum, and the solid curve is the theoretical curve of Fig. 10 normalized to the experimental counting rate at 0°.

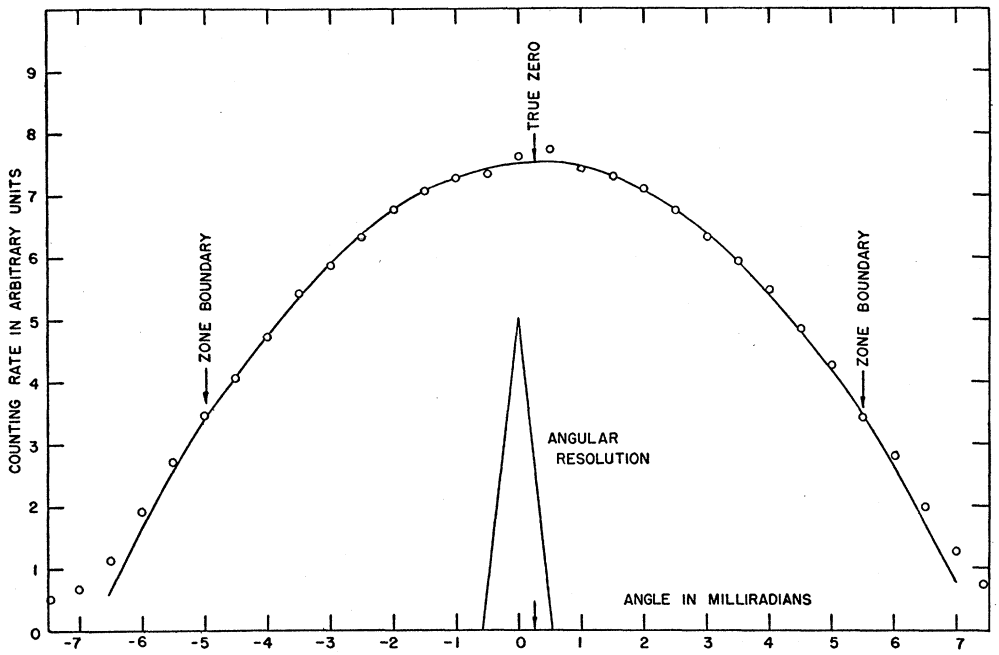

FIG. 13. Experimental angular distribution in Al oriented along the [111] direction [momenta perpendicular to the (111) plane]. The solid curve is a parabola fitted to the experimental points as described in the text. The boundary of the Brillouin zone is indicated.

tails as computed in Sec. 4.3 superimposed on an isotropic distribution due to the M-shell electrons. A comparison between any of the three curves on Fig. 11 and the theoretical curve for Cu of Fig. 9 shows that the theory overestimates the M-shell contribution. A doubling of the theoretical parabola contribution would give a good fit to the experimental data. This effect could be then attributed to a somewhat stronger correlation with the valence electrons than with the M electrons. A slight change in the computed positron wave function would, however, easily introduce the same desired effect; we have seen how sensitive the momentum distribution is to the shape of the positron wave function in Sec. 4. (Compare ρ_{3d} with ρ_{3d}' in Fig 3.) Such a change in the positron wave function could result, for example, from a cellular computation instead of the Wigner-Seitz method used in this paper.

In Fig. 12 we plot the measured angular distribution of aluminum (the [111] direction) and compare it to the theoretical curve of Fig. 10 normalized to the experimental counting rate at 0° (in arbitrary units). The agreement between theory and experiment as regards the shape and magnitude of the high-momentum component in Al is excellent. The experimental points were taken with a 0.56-milliradian slit opening at intervals of 0.5 milliradian.

Finally it may be asked whether deviations of the Fermi surface from a sphere can be detected by variations of the position of the cutoff in the angular distribution corresponding to measuring a component of momentum in different directions. Also the exact shape of the distribution would reflect such an anisotropy. This is clearly very difficult in the case of copper or any other metal that exhibits a strong high-momentum distribution. We have concentrated therefore to measure more precisely the shape of the Al distribution, where the tail has but a small effect on the central "parabola". The question was: how will the experimental points fit a parabola and to what extent are there deviations along different orientations? In Figs. 13 and 14 we have plotted the distributions obtained from -7 to $+7$ mrad in steps of 0.5 mrad for the [111] and [100] directions. It can be easily shown that if one folds a parabola with a cutoff into a triangular resolution of base λ, the resulting curve deviates from a parabola only within $\lambda/2$ from the cutoff angle. We have performed a least-squares fit to the experimental points between -5 mrad and $+5$ mrad using the method of orthogonal polynomials.[20] The result of this computation clearly indicated that the data can be fitted well (within the statistical variation of the individual points —one percent) by a parabola, after automatically obtaining the true zero of the distribution. These parabolas are also plotted on Figs. 13 and 14. Using the theoretical value of the contribution of the L shell distribution one obtains for the cutoff angles 6.88 mrad and 7.02 mrad for the [111] and [100] directions. These angles are to be compared with 6.767 mrad computed from the free electron model. Along the [100] direction the Fermi surface seems to be bulged out by about 4%. This result is in qualitative agreement with the conclusions of Heine[21] on the Fermi surface in Al. We estimate the precision of these experimental cutoffs to be about 1–2%.

The arrows on the curves of Figs. 13 and 14 indicate

[20] R. T. Birge, Revs. Modern Phys. **19**, 298 (1947).
[21] V. Heine, Proc. Roy. Soc. (London) **A240**, 340 (1957).

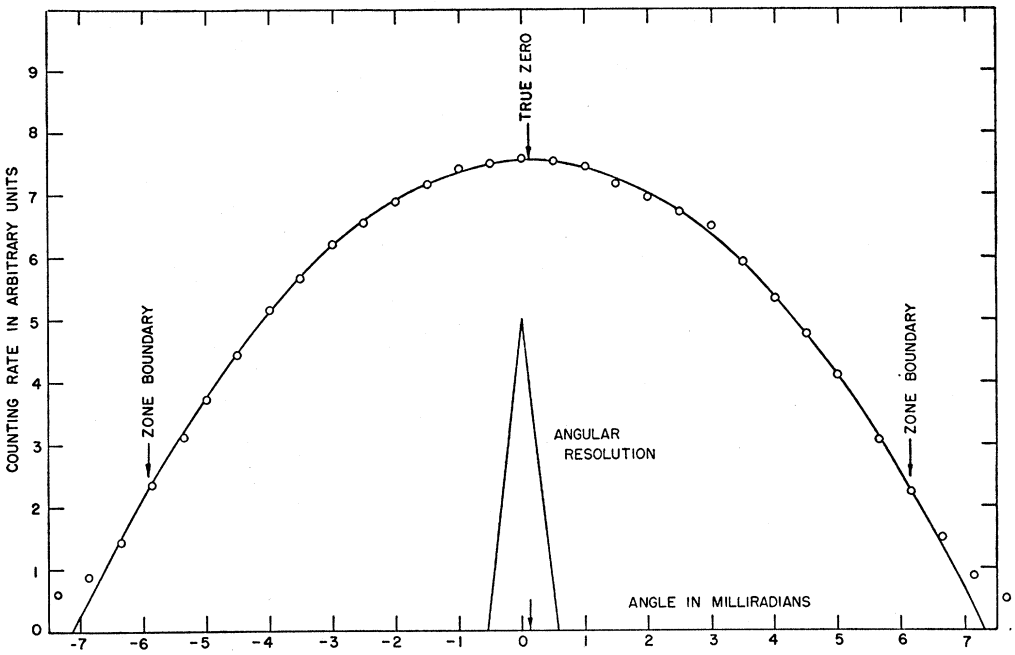

FIG. 14. Experimental angular distribution in Al oriented along the [100] direction [momenta perpendicular to the (100) plane]. The solid curve is a parabola fitted to the experimental points as described in the text. The boundary of the Brillouin zone is indicated.

the position of the Brillouin zone faces. There seems to be an indication that the experimental points deviate from the central parabola slightly along the [111] direction starting at the zone boundary, but this qualitative deviation will have to be studied much more thoroughly with better angular resolution.

That the combined momentum distribution of the two bands in aluminum is just the same as for free electrons, that nothing violent happens to the momentum distribution on going through a zone face, and that there is not a break in the angular distribution corresponding to the Fermi surface in the reduced zone scheme, may seem odd. We gave a rough explanation of these peculiarities in terms of the nearly free electron approximation in Sec. 4. We have also shown that the angular distribution will not have a sharp cutoff at a zone face if the Fermi surface happens to coincide with a portion of the zone face. The momentum distribution extends beyond the zone face to a distance proportional to the enery gap in the zone face. This explains why insulators never have a sharp cutoff and should enable one to determine on which zone face there is overlap and on which there is contact if the angular resolution can be made sufficiently small (probably better than $\frac{1}{2}$ mrad for energy gaps of the order of 0.15 ry).

In their paper on the importance of positron-electron correlation, Friedel and Daniel predict deviations from a parabola in the angular distribution near low momenta. In order to search for such a deviation, we have made a separate run in the region from -2.5 mrad to $+2.5$ mrad in Al, and have accumulated at each 0.5 mrad 20 000 counts. We found that within this precision (0.7%) the experimental points fall on a parabola.

Further measurements are in progress on oriented metal crystals, with improved resolution and higher counting rates due to a larger Na^{22} source. It is obvious that hexagonal crystals have a greater promise to show anisotropies than the cubic metals discussed in this paper. In view of our discussion, however, it is evident that it will be hard to detect effects of the shape of the Fermi surface in metals that exhibit large momenta distributions due to annihilation with core electrons.[22] A paper describing measurements on oriented Mg will follow shortly.

[22] This might be the reason for the negative results presented recently by Lang on Cd crystals: L. G. Lang and N. C. Hien, Phys. Rev. **110**, 1062 (1958).